


Chemical abundances of the high-latitude Herbig Ae Star PDS2

C. R. Cowley¹ *, S. Hubrig², and N. Przybilla³

¹*Department of Astronomy, University of Michigan, Ann Arbor, MI 48109-1042, USA*

²*Leibniz-Institut für Astrophysik Potsdam (AIP), An der Sternwarte 16, 14482, Potsdam, Germany*

³*Institute für Astro- und Teilchen Physik, Technikerstr. 25/8, A-6020 Innsbruck, Austria*

Accepted . Received ; in original form

ABSTRACT

The Herbig Ae star PDS2 (CD -53° 251) is unusual in several ways. It has a high Galactic latitude, unrelated to any known star-forming region. It is at the cool end of the Herbig Ae sequence, where favorable circumstances facilitate the determination of stellar parameters and chemical abundances. We find $T_{\text{eff}} = 6500$ K, and $\log(g) = 3.5$. The relatively low $v \cdot \sin(i) = 12 \pm 2$ km s⁻¹ made it possible to use mostly weak lines for the abundances. PDS2 appears to belong to the class of Herbig Ae stars with normal volatile and depleted involatile elements, thus resembling the λ Boo stars. The intermediate volatile zinc consistently violates this pattern.

Key words: –stars:Herbig Ae –stars:abundances –stars:individual: PDS2 –stars:individual: HD 104237 –stars:individual: HD 101412 –stars:individual: HD 190073

1 INTRODUCTION

Gregorio-Hetem, et al. (1992) describe their survey of stars in the IRAS Point Source Catalog (1988) for T Tauri stars. Their work and follow-up studies became known as the Pico dos Dias Survey (PDS). It located a number of Herbig Ae/Be candidates, among them the isolated, high-latitude object, PDS2 (CD -53 251). Subsequent studies (e.g. Vieira, et al. 2003, Pogodin et al. 2012) confirmed the classification as a young stellar object. The δ Scuti-like pulsations discovered by Bernabei, et al. (2007) were confirmed by Marconi et al. (2010), who noted that it could “constrain the poorly sampled red edge of the PMS [pre main sequence] instability strip.” The presence of a weak magnetic field in this star is uncertain, as the star was observed only on two different epochs (Wade, et al. 2007, Hubrig et al. 2009). Bagnulo, et al. (2012) conclude that a field is possible, but “certainly not yet definitely established.”

The metallic-line (absorption) spectrum of PDS2 is well developed, as its temperature places it among the mid F-type stars. Emission is restricted to the hydrogen and helium lines and [O I].

The PDS2 spectrum has relatively sharp lines, which enables us to use weak lines whose equivalent widths are independent of instrumental or rotational broadening. This is not the case for many Herbig Ae stars.

Table 1. Observations. See text for explanation and references.

Spectrum	epoch(JD245)	S/N	$\lambda/\Delta\lambda$
HARPS	4781.08/4782.04	~45	~60000
X-shooter	5375.5	550	~17400
CRIRES	6153.5/6172.5	175	~90000

The youth of PDS2 and its high Galactic latitude pose the question of whether the star was born close to the Galactic plane. The available kinematical data are not precise enough to answer this question unequivocally.

This paper may be considered a sequel to three previous abundance studies of the Herbig Ae stars HD 101412, HD 190073, and HD 104237 (Cowley et al. 2010, Cowley & Hubrig 2012, and Cowley et al. 2013). We refer to them as Papers I, II, and III, respectively.

2 OBSERVATIONAL MATERIAL

The observational materials are summarized in Table 1. Note that the entries for signal to noise (S/N), and resolving power (RP or $\lambda/\Delta\lambda$) are typical values. Individual measurements can vary by as much as 30%. Resolution and S/N for X-shooter are from Pogodin et al. (2012), for CRIRES from Cowley, et al. (2012).

* E-mail: cowley@umich.edu

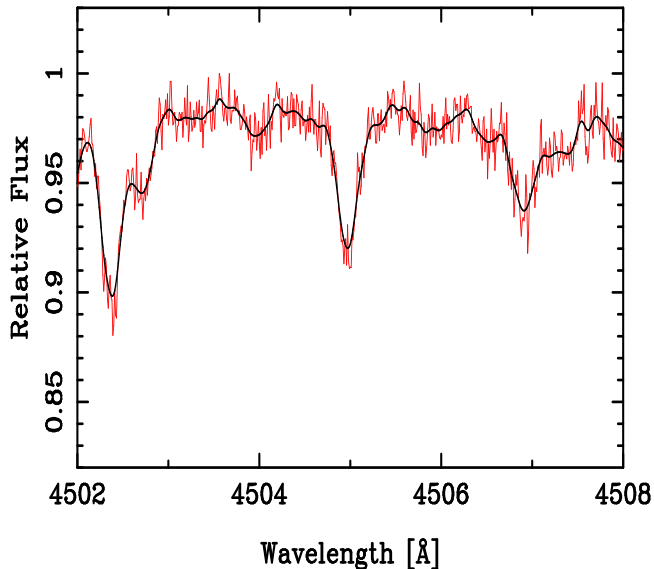


Figure 1. Sample region showing averaged (gray/red online) and Fourier filtered (black) spectrum.

Equivalent width measurements were made on 9 averaged HARPS (Mayor, et al. 2003) spectra downloaded from the ESO archive. We examined two sets of 9 spectra obtained on the nights of 11/12 November and 13 November 2008 UT. The first set of spectra were clearly of higher quality than the second, and all measurements were therefore based on that set. The largest difference in barycentric radial velocities found in the fits headers for the adopted spectra was 0.079 km s^{-1} . We attempted to allow for the differences in radial velocity, but the results were no better than straight averages, which we adopted.

To find the signal-to-noise ratios, we fit second-order curves to portions of the spectra that appeared to be free of absorption lines, or contained the smooth wing of a strong line. The S/N is taken to be the standard deviation of points from these fits.

The added spectra were still noisy, and were Fourier filtered using the standard Brault-White (1971) algorithm. Typical values of S/N for one of the individual exposures are ~ 45 . After addition the S/N increases to typically ~ 130 . Filtering further reduces the unwanted, high-frequency power by a factor of ~ 2.5 , to ~ 320 , as illustrated in Fig. 1. The latter value is strictly not S/N as the filtered points are correlated.

The resolution of the averaged and filtered spectrum is about 60,000, based on fits of gaussians to telluric lines, and the sharp, stellar [O I] (see Sec. 4).

For the O I triplet, outside the HARPS coverage we used an X-shooter (Vernet, et al. 2011) spectrum. A CRIRES (Käufl, et al. 2004) spectrum is used to show the He I $\lambda 10830$ emission.

3 NORMALIZATION AND EQUIVALENT WIDTHS

Normalization of the spectrum is done with a code written by CRC. The spectrum is viewed in 80 \AA intervals, and high points are located approximately with a cursor. In a second

pass, the actual highest points are found within 0.5 \AA of the initially chosen points. Finally, the continuum is chosen to pass through these points using a weighted combination of linear interpolation and a cubic spline fit.

It is generally known that the wide profiles of the Balmer lines are difficult to obtain from echelles, such as HARPS or UVES. Our normalization procedure was a standard one. Perhaps the intrinsically narrower profiles of a mid-F star makes the echelle order gap merging less troublesome. In any case, we have obtained good agreement with the wing calculations and the observed profiles of $H\beta$, $H\gamma$ (Figure 6) and $H\delta$ from *both* instruments (HARPS and X-shooter). With the exception of the $H\alpha$ profile (Figure 4), no adjustments to the observed profiles were necessary to achieve good agreement with the calculations.

Equivalent widths are measured individually, using Voigt profile fits, as in previous studies (Papers I - III). The smallest equivalent width used in this paper was 4.2 m\AA . Features of the order of 1 or 2 m\AA cannot be positively distinguished from noise.

4 THE SPECTRUM OF PDS2

Most of the spectrum of PDS2 is typical of a mid-F star. There are no metallic emission lines, which are common in the spectra of young stars. Emission at $H\alpha$ and He I $\lambda 10830$, in addition to the infrared excess found in the IRAS survey are the basis of the assignment of PDS2 to the class of young stars.

The rotational velocity was determined from the synthesis of numerous stellar features (e.g. Mg II $\lambda 4481$). We conclude this star has a relatively low $v \cdot \sin(i)$, $12 \pm 2 \text{ km s}^{-1}$. This assumes that the macroturbulence has a negligible half-width relative to the rotational half-width. The $v \cdot \sin(i)$ could be lower if the macroturbulence were of comparable value. The distinction is of little consequence for abundances based almost exclusively on equivalent widths.

Figure 2 compares a region of the spectra of 4 Herbig Ae stars. They are arranged in order of increasing importance of metallic emission lines.

Interestingly, sharp, [O I] lines are seen in emission, displaced some $25\text{-}30 \text{ km s}^{-1}$ to the violet (Fig. 3). The violet portion of the $\lambda 6300$ line is absorbed by an atmospheric and/or stellar feature, so an accurate velocity cannot be determined. Similar sharp [O I] emissions were noted in HD 190073 (Paper II) with a comparable shift. He I, $\lambda 5876$ is also weakly in emission.

Apart from $H\alpha$ (Figure 4) and He I $\lambda 10830$ (Figure 5) there are no strong emissions in our spectra of PDS2. Both lines are variable. See Hubrig, et al. (2013) for variability of $\lambda 10830$. Pogodin, et al. (2012) measured equivalent widths at 8 phases for of $H\alpha$ and He I $\lambda 5876$ from their X-shooter spectra. Emissions at $P\beta$, $P\gamma$ and $Br\gamma$ were measured at 5 phases. These features were used to determine mass accretion rates. For PDS2, they found $\log(\dot{M}_{\text{acc}}) = -8.68$ in $M_{\odot} \text{ yr}^{-1}$.

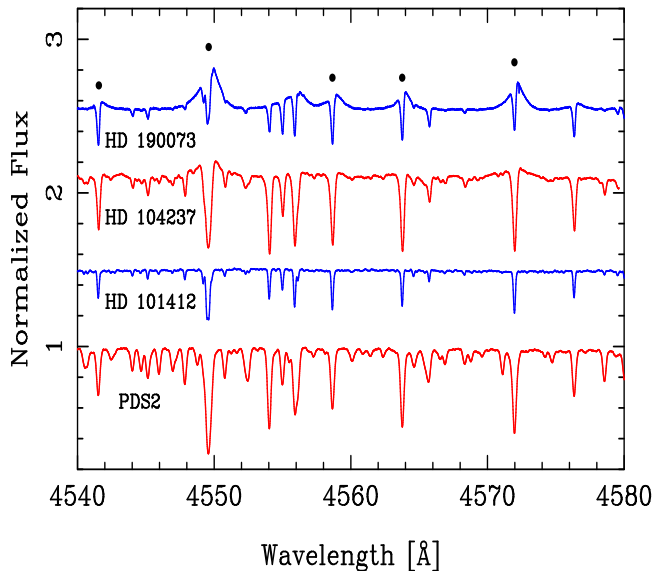


Figure 2. Sample spectra of four Herbig Ae stars. Filled circles mark metallic lines sometimes in emission. HD 190073 has the most developed metallic emissions, followed by HD 104237 (DX Cha). No emissions are seen in this region of the HD 101412 spectrum, or PDS2. The top 3 spectra were discussed in Papers I, II, and III.

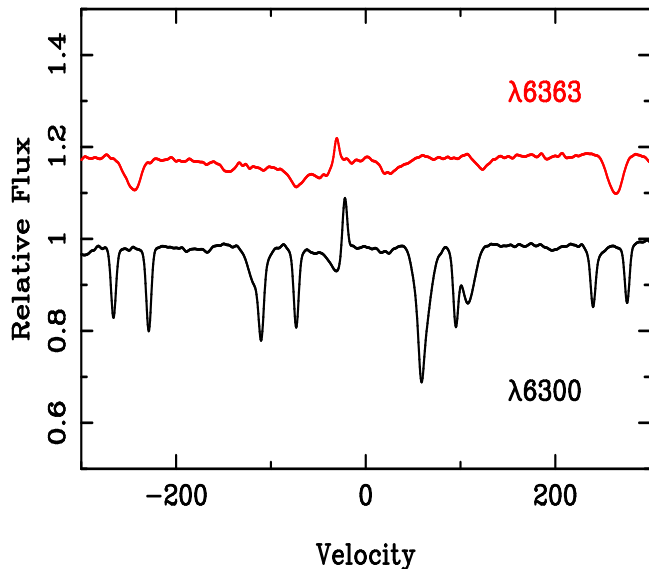


Figure 3. Emissions near [O I] rest wavelengths (Velocity = 0). The $\lambda 6363$ region (gray/red online) has been shifted upward for purposes of display. Both emissions are displaced to the violet with respect to the stellar lines. The stronger line appears slightly less displaced because of absorption on its violet edge.

5 ATMOSPHERIC PARAMETER DETERMINATION

5.1 Model atmosphere and spectral codes

The model atmosphere code used here adopts the $T(\tau)$ relation from an ATLAS9 (Kurucz 1993, Castelli & Kurucz 2003) calculation assuming solar abundances from the

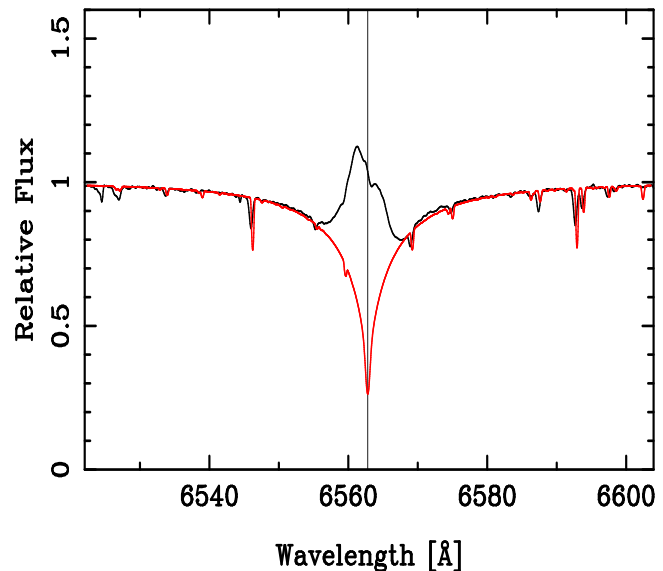


Figure 4. H α from the X-shooter spectrum. The observed continuum (black) has been lowered by 1% for optimum fit (gray/red online) to the line wings.

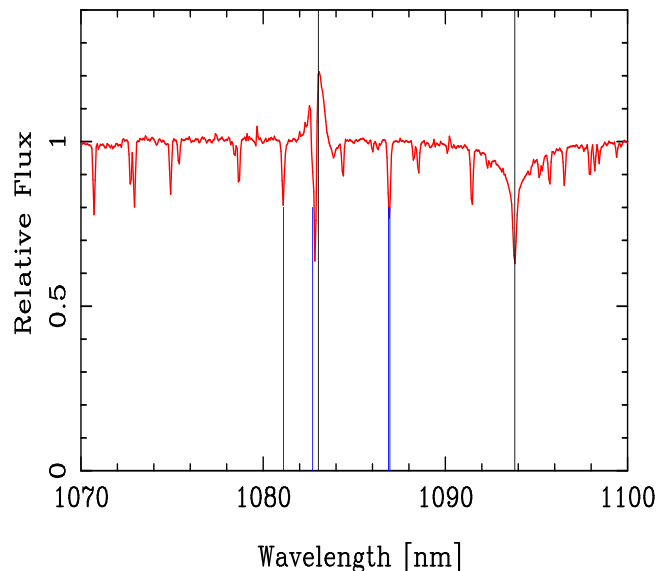


Figure 5. CRILES spectrum showing He I $\lambda 10830$ in emission, and P γ $\lambda 10938$ in absorption. Vertical lines mark rest wavelengths; shorter lines are for Mg I (10811.05 Å) and Si I (10827.09, 10868.79, and 10869.54 Å). The remaining sharp absorptions are telluric or unidentified.

Castelli website¹). The depth integrations are carried out by a code written at Michigan, using (PDS2) abundances. We believe that the resulting minor inconsistency between the adopted $T(\tau)$ and $P(\tau)$ has no significant influence on the abundance determination presented below.

The atomic hydrogen and helium opacities are from Kurucz. For H⁻, we used an interpolation formula in Gray (2005). Topbase opacities are implemented for other elements, as described by Cowley, et al. (2003). These opacities

¹ wwwuser.oat.ts.astro.it/castelli/

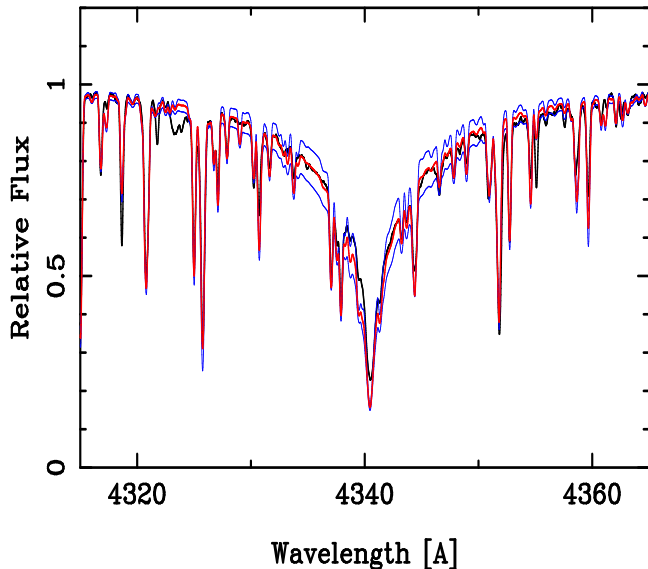


Figure 6. Averaged and filtered HARPS spectrum of $H\gamma$ (black). The gray (red online) spectrum is synthesized with the adopted model. The thin lines (blue online) show synthesized spectra with temperatures ± 250 K from the adopted 6500 K model. Molecular features were not included in the synthesis, which accounts for some of the absorption not in the calculation, e.g. the CH lines near $\lambda 4323$ – 4325 .

are also used in the synthesis codes, which carry out flux integrations, which are then convolved with rotational profiles, as described, for example, by Gray (2005). Equivalent width calculations are usually of one line only; occasionally a close-line pair will be synthesized, and the combined equivalent width used for an abundance. Apart from oxygen, only Co I, $\lambda 4867.9$ was synthesized because of its location near $H\beta$. The oxygen calculation is described separately below (Section 6.1).

The methods used here are the same as in Papers I–III. Results from our codes have been verified by coauthors using independent codes, and in independent studies (e.g. Folsom, et al. 2012, 2013).

5.2 Balmer lines

It is well known that the strengths of the Balmer lines are highly sensitive to the effective temperatures of stars later than the early F’s. In the temperature range of interest here, 6500 ± 150 K, there is at most a few per cent difference in the profiles with $\log(g)$ from 4.0 to 3.5, the latter being the relevant range of surface gravities.

The $H\beta$ profiles of both the HARPS and X-shooter spectra (not shown) have cores that are slightly less deep than the calculations. The violet edges of the cores are also stronger than the calculated profiles. The Balmer emission in PDS2 is variable, as has been discussed, for example, by Pogodin, et al. (2012).

The $H\gamma$ and $H\delta$ profiles of PDS2 are hardly distinguishable from those of Procyon—apart from the stronger metallic lines in the latter star. Most recent work puts the effective temperature of Procyon between 6500 and 6600 K (Liebert, et al 2013, Boyajian, et al. 2013). A calculated $H\gamma$ profile for PDS2 with $T_{\text{eff}} = 6600$ K is slightly too strong, though

possibly acceptable. A model with $T_{\text{eff}} = 6700$ K is not acceptable. If the temperature were as high as 6750 K, the abundance from an Fe I line with a typical excitation of 2.2 eV would increase by 0.15 dex.

5.3 Metal lines, gravity, turbulence, and abundances

Generally, one may obtain a relation between the effective temperature and surface gravity of a star from the strengths of lines from neutral and first-ionized atoms, e.g. Fe I and II. In the temperature range that we have found for PDS2, the strengths of Fe I lines are virtually independent of surface gravity (see Gray 2005). If the lines are weak, say < 20 mÅ, their equivalent widths are also independent of broadening mechanisms.

We have used equivalent widths of *weak* Fe I to directly determine the iron abundance in PDS2. The microturbulence (ξ_t) may then be determined from intermediate and strong Fe I lines.

Equivalent widths, abundances, wavelengths, and excitation potentials for all atomic and ionic species with more than 6 lines are read into a spreadsheet. Plots are then made of the abundance vs. equivalent width, excitation potential, and wavelength. The microturbulence is chosen to minimize the dependence of abundance on line strength. We adopted the $\xi_t = 1.8$ km s $^{-1}$, first obtained for Fe I, the spectrum with the most lines. This value was compatible with other spectra with numerous weak and strong lines, e.g. Cr I, Cr II, etc. Because most of the lines used for abundance were weak, results are not sensitive to this parameter.

The surface gravity is then chosen to make abundances from neutral and first-ionized species agree.

The weakest links in this chain of deduction for the atmospheric parameters are the absolute oscillator strengths of the relevant species. Our choices for the oscillator strengths are given in Paper III and in the online material.

We tabulate abundances based on a model with $T_{\text{eff}} = 6500$ K. The $\log(g) = 3.5$, but we estimate a range of 3.75–3.3. Most of the metal abundances, based on the first spectra, are insensitive to gravity uncertainties in this range.

6 ABUNDANCES

6.1 Oxygen (NLTE)

For the determination of oxygen abundances from the strong O I $\lambda\lambda 7771$ – 5 Å near-IR triplet or from O I $\lambda 8446$ Å, non-LTE effects need to be accounted for. We employed updated and extended versions of the DETAIL/SURFACE codes (Giddings 1981; Butler & Giddings 1985) for non-LTE line-formation computations on the prescribed model atmosphere. The O I model atom of Przybilla et al. (2000) was used. This was extended to account for collision strengths for electron impact excitation by Barklem (2007), excitation and ionization due to hydrogen collisions employing the Steenbock & Holweger (1984) approximation (adopting a scaling factor $S_H = 1$, determined from fitting the solar oxygen spectrum). Background opacities appropriate for mid-F-type stars are from Przybilla & Butler (2004), with some improvements. Line blocking is considered via the LTE opacity sampling

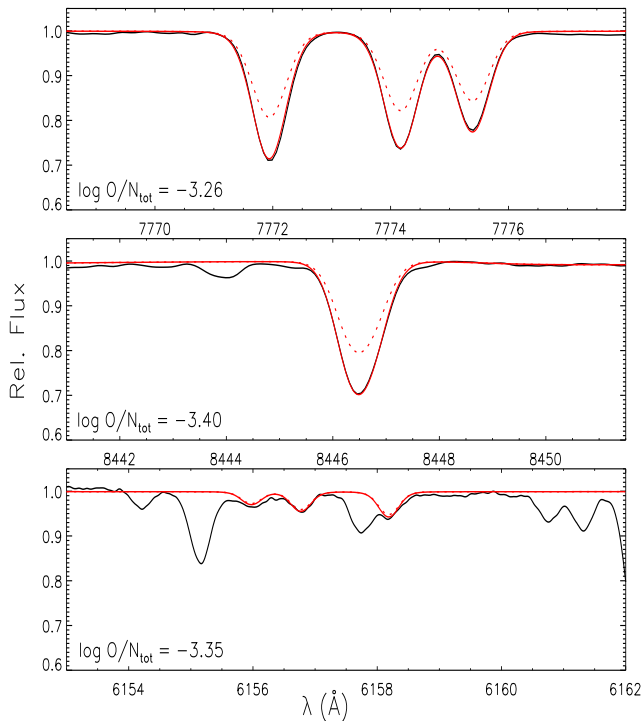


Figure 7. Spectrum synthesis of the observed O I lines (black), in non-LTE (full gray/red(online) lines) and LTE (dotted gray/red lines). Best-fit abundances for the multiplets are indicated. Note that only O I λ 6156.7 Å was considered for the abundance determination in the lower panel, because of the blending of the other components.

technique according to Kurucz (1996). The van der Waals broadening coefficients are from Barklem et al. (2000). Figure 7 shows the best fits to the observed O I multiplets. LTE line profiles for the same abundances are indicated for comparison. The non-LTE abundance corrections are essential, amounting to about -0.6 to -0.8 dex for the stronger lines. From the weak O I λ 6155-8 Å triplet only the component at 6156.7 Å was considered for the abundance determination because of the strong blends in the other lines. Blends of O I λ 8446 Å with the weak Fe I λ 8446.39/.57 Å lines were accounted for, adopting our mean Fe I abundance.

Oscillator strengths for λ 7771-5 and 8446 are from Froese Fischer & Tachiev (2004). Those for λ 6155-8 are from Wiese, Fuhr & Deters (1996).

6.2 LTE for other elements

Some studies have given NLTE corrections (cf. Hansen, et al. 2013), and for dwarfs near solar abundances, they are rather small for Fe I, less than 0.1 dex (see their Fig. 2). A study by Mashonkina, et al. (2011) discusses NLTE effects in Procyon (Table 3). Abundance results differ from LTE by values under 0.03 dex, and might be zero, depending on assumptions made about collisional rates with atomic hydrogen. An additional indication that LTE is a reasonable approximation is that our abundances based on first and second spectra are in good agreement, usually better than 0.1 dex.

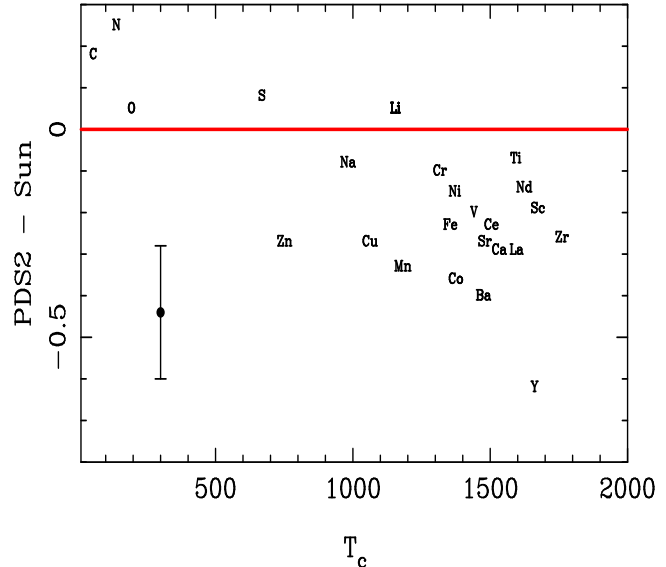


Figure 8. Logarithmic abundance differences between PDS2 and the solar photosphere vs. condensation temperatures T_c from Lodders(2003). Data points are the lower left corner of the chemical symbols. An average error bar is shown at the lower, left corner. Individual values are in Table 2

6.3 Discussion of the results

Table 2 gives abundances in PDS2 and the Sun as logarithms. The 50% condensation temperatures (T_c), indicative of volatility, are from Lodders (2003). We find no evidence of the presence of Li I λ 6707, and report only an upper limit. Entries are given for several species that are obviously present, but for which suitable weak lines were unavailable. These cases are indicated by ‘n.u.’ for “not used.” Probable errors (pe) are usually standard deviations of the abundances from ‘ n ’ lines. When $n = 2$, we used the difference between the values, except when that difference was unrealistically small, in which case a rough estimate is entered. Solar abundances are from Asplund, et al.(2009).

Results of wavelength coincidence statistics or WCS (Cowley & Hensberge 1981) indicate that lines of Pr II and Gd II are present at 0.02 and 0.009 significance (or false alarm probability) levels. The certain presence of Ce II and Nd II leads us to believe Pr II and Gd II are indeed present, though weak and blended. We found no usable lines for an abundance estimate.

Equivalent widths, oscillator strengths, and abundances are available in the online material for some 318 absorption lines.

Figure 8 shows a depletion of volatile elements with respect to the Sun in PDS2. Unlike a similar result with HD 101412 (Paper I), the correlation of depletion with condensation temperature appears monotonic—admittedly with considerable scatter. Note that the intermediate volatile zinc is depleted, unlike the general trend. Folsom, et al. (2012) define a peculiarity index,

$$[P] = \frac{1}{3}([Cr] + [Fe] + [Ni] - [C] - [N] - [O]), \quad (1)$$

which is a measure of the refractory depletion and the non-depletion (or excesses) of the volatiles.

We find $[P] = -0.31$, which places PDS2 among the

Table 2. Adopted abundances. Column 2 is the condensation temperature from Lodders (2003). The number of lines used is in the column labeled *n*. Probable errors are in Column 4.

Spec	T_c	$\log(El/N_{\text{tot}})$	$\pm pe$	<i>n</i>	Sun
Li I	1135	≤ -10.95		1	
C I	40	-3.44	0.14	7	-3.61
N I	123	-3.97	0.23	2	-4.21
O I	179	-3.31	0.07	5	-3.35
Na I	953	-5.89	0.10	4	-5.80
Mg I	1327	-4.48	0.14	2	-4.44
Mg II		n.u.			
Al I	1641	-5.92	0.20	2	-5.59
Si I	1302	-4.69	0.30	7	-4.52
Si II		n.u.			
S I	655	-4.85	0.06	6	-4.92
Ca I	1505	-6.00	0.16	7	-5.70
Ca II		n.u.			
Sc II	1647	-9.18	0.11	5	-8.98
Ti I		-7.09	0.15	6	
Ti II		-7.21	0.08	3	
Ti	1573	-7.17	0.15		-7.09
V I		-8.32	0.07	5	
V II		-8.39	0.14	3	
V	1427	-8.32	0.07		-8.11
Cr I		-6.52	0.31	12	
Cr II		-6.49	0.26	11	
Cr	1291	-6.51	0.29		-6.40
Mn I	1150	-6.95	0.19	15	-6.61
Mn II		n.u.			
Fe I		-4.79	0.08	10	
Fe II		-4.76	0.13	17	
Fe	1328	-4.78	0.10		-4.54
Co I	1347	-7.42	0.02	2	-7.05
Ni I	1348	-5.98	0.12	16	-5.82
Ni II		n.u.		2	
Cu I	1033	-8.12	0.34	2	-7.84
Zn I	723	-7.76	0.13	3	-7.48
Sr II	1455	-9.45	0.1	2	-9.17
Y II	1647	-10.46	0.12	6	-9.83
Zr II	1736	-9.73	0.21	4	-9.46
Ba II	1447	-10.27	0.3	2	-9.86
La II	1570	-11.24	0.12	4	-10.94
Ce II	1477	-10.70	0.14	5	-10.46
Nd II	1594	-10.77	0.32	2	-10.62

typical types of the Folsom, et al. study with negative [*P*] indices.

7 GENERAL REMARKS

The similarity of the abundance peculiarities of some Herbig Ae and those of the λ Boo stars is becoming firm. We have now studied 4 Herbig Ae stars with relatively sharp lines. Two have shown the noted peculiarities, while two have not. These results match those of the broader survey of Folsom, et al (2012), who concluded “half the stars in our sample show λ Boo chemical peculiarities to varying degrees.” Their work included HD 101412 and HD 190073. They found the former star to have λ Boo-like, and the later to have solar abundances, as we reported in Papers I and II.

The connection between young stars and λ Boo abundances was noted by Gray and Corbally (1998), whose mono-

graph (Gray and Corbally 2009) contains a description of λ Boo and Herbig Ae/Be stars, as well as theories of their origin. These authors and others (e.g. Heiter, et al. 2002) note that this general pattern—the selective depletion of refractory elements—occurs in certain RV Tauri and post-AGB stars, objects with vastly different structure and evolutionary history from Herbig Ae stars.

More recently (cf. Meléndez 2013), precision abundances of the Sun and solar-like stars have revealed a similar pattern of depletion of refractory elements in the Sun itself.

The most common explanations of how these abundance patterns arise have built on the suggestions of Venn and Lambert (1990). They noted the similarity of the λ Boo abundances to those of the interstellar gas from which refractory elements have been lost due to depletion onto grains. The grain-gas separation could take place in interstellar or circumstellar environments. Meléndez (2013) has suggested the sun’s depletion of refractory elements is due to the formation of (metal/rocky) terrestrial planets. Quite different models may be required for the diverse objects that share the pattern of refractory-element depletions. But all are likely to draw upon the chemo-thermodynamic properties of the elements.

The Herbig Ae stars, must represent the progenitors of normal A stars. However, since half of these young A-stars are chemically peculiar, some explanation of how the older stars become normal or metal rich is required. The ages of λ Boo stars are quite uncertain due to their near absence in galactic clusters. The Herbig Ae stars, however, are definitely young. It is plausible that their abundance anomalies can be destroyed by diffusion or meridional mixing, as suggested by Turcotte (2002).

8 ACKNOWLEDGEMENTS

We thank J. R. Fuhr, J. Reader, and W. Wiese of NIST for advice on atomic data and processes, and J. F. González for help with the observational material. This research has made use of the SIMBAD database, operated at CDS, Strasbourg, France. Our calculations have made extensive use of the VALD² atomic data base (Kupka, et al. 1999), as well as the NIST³ online Atomic Spectroscopy Data Center (Kramida, et al. 2013). CRC is grateful for advice and helpful conversations with many of his Michigan colleagues. He thanks Jesus Hernández for a discussion of the status of PDS2, and C. Folsom for a useful email exchange on the possible chemical evolution of Herbig Ae stars.

This research is based archival data from observations obtained at the European Southern Observatory, Paranal and La Silla, Chile (ESO programmes 082.D-0833(A), Archive request Nos. 54506 SAF and 59603 SAF).

REFERENCES

Asplund, M., Grevesse, N., Sauval, A. J., Scott, P. 2009, *Ann. Rev. Astron. Ap.* 47, 481

² <http://vald.astro.univie.ac.at/~vald/php/vald.php>

³ <http://www.nist.gov/pml/data/index.cfm>

- Bagnulo, S., Landstreet, J. D., Fossati, L. & Kochukhov, O. 2012, *A&A*, 538, 129
- Barklem, P.S. 2007, *A&A*, 462, 781
- Barklem, P.S., Piskunov, N., O'Mara, B.J. 2000, *A&AS*, 142, 467
- Bernabei, S., Marconi, M., Ripepi, V., Leccia, S., Rodríguez, E., Oswalt, T. D., et al. 2007, *Comm. in Asteroseismology*, 150, 2007
- Boyajian, T. S., von Braun, K., van Belle, G., Farrington, C., Schaefer, G., Jones, J., et al. 2013, *ApJ*, 771, 40
- Brault, J. W. & White, O. R. 1971, *A&A*, 13, 169
- Butler, K., & Giddings, J.R. 1985, in *Newsletter of Analysis of Astronomical Spectra*, No. 9 (Univ. London)
- Castelli, F. & Kurucz, R. L. 2003, in *Modelling of Stellar Atmospheres*, ed. N. Piskunov, W. W. Weiss, D. F. Gray, IAU Symposium 210, (A 20) p. 424
- Cowley, C. R., Adelman, S. J. & Bord, D. J. 2003, in *Modelling of Stellar Atmospheres*, ed. N. Piskunov, W. W. Weiss, & D. F. Gray (IAU Symposium 210), p. 261
- Cowley, C. R. & Hensberge, H. 1981, *ApJ*, 244, 252
- Cowley, C. R., Hubrig, S., González & Savanov, I. 2010, *A&A*, 523, 65 (Paper I)
- Cowley, C. R. & Hubrig, S. 2012, *AN*, 333, 34 (Paper II)
- Cowley, C. R., Hubrig, S., Castelli, F. & Wolff, B. 2012, *A&A*, 537, L6
- Cowley, C. R., Castelli, F. & Hubrig, S. 2013, *MNRAS*, 431, 3485 (Paper III)
- Folsom, C. P., Bagnulo, S., Wade, G. A., Alecian, E., Landstreet, J. D., Marsden, S. C. & Wate, I. A. 2012, *MNRAS*, 422, 2072
- Folsom, C. P., Bagnulo, S., Wade, G. A., Landstreet, J. D. & Alecian, E. 2013, *Magnetic fields throughout stellar evolution*, *Proc. IAU Symp.* 302, ed. P. Petit, arXiv:1311.1552
- Froese Fischer, C., & Tachiev, G. 2004, *At. Data Nucl. Data Tables*, 87, 1
- Giddings, J.R. 1981, Ph.D. Thesis (Univ. London)
- Gray, D. F. 2005, *The Observation and Analysis of Stellar Photospheres*, 3rd ed. (Cambridge: University Press, see p. 322)
- Gray, R. O., & Corbally, C. J. 1998, *AJ*, 116, 2530
- Gray, R. O. & Corbally, C. J. 2009, *Stellar Spectral Classification* (Princeton: Series in Astrophys.), see pp. 199–203
- Gregorio-Hetem, J., Lépine, J. R. D., Quast, G. R., Torres, C. A. O. & de la Reza, R. 1992, *AJ*, 103, 549
- Heiter, U., Weiss, W. W. & Paunzen, E. 2002, *A&A*, 381, 971
- Hansen, C. J., Bergemann, M., Cescutti, G., Francois, P., Arcones, A., Karakas, A. I., et al. 2013, *A&A*, 551, 57
- Hubrig, S., Stelzer, B., Schöller, M., Grady, C., Schütz, Pogodin, M. A., et al. 2009, *A&A*, 502, 283
- Hubrig, S., Illyn, I., Cowley, C. R., Castelli, F., Stelzer, B., et al. 2013, arXiv:1308.6777 (to appear in *Proceedings of the Conference "Physics at the Magnetospheric Boundary"*, EDP Sciences, in press.
- IRAS Science Team, 1988, *Catalogs and Atlases*, Vol. 2–6: *The Point Source Catalog (PSC)*, ed. Beichman, C. A., Neugebauer, G., Habing, H. J., Clegg, P. E. & Chester, T. J., NASA RP-1190
- Käuffl, H.-U., Ballester, P., Biereichel, P., Delabre, B., Donaldson, R., Dorn, R., et al. 2004, *SPIE*, 5492, 1218
- Kramida, A., Ralchenko, Yu., Reader, J., and NIST ASD Team (2013). *NIST Atomic Spectra Database* (ver. 5.0), [Online]. Available: <http://physics.nist.gov/asd> [2013, February 21]. National Institute of Standards and Technology, Gaithersburg, MD.
- Kupka, F., Piskunov, N. E., Ryabchikova, T. A., Stempels, H. C., Weiss, W. W. 1999, *A&AS*, 138, 119
- Kurucz, R. L. 1993, *ATLAS9 Stellar Atmosphere Programs and 2 km/s grid*, CD-Rom, No. 13, Cambridge MA: Smithsonian Ap. Obs.
- Kurucz, R. L. 1996, in *Model atmospheres and spectrum synthesis*, ASP Conf. Ser. 108, ed. S. J. Adelman, F. Kupka & W. W. Weiss, p. 160
- Liebert, J., Fontaine, G., Young, P. A., Williams, K. A. & Arnett, D. 2013, *ApJ*, 769, 7
- Lodders, K. 2003, *ApJ*, 591, 1220
- Marconi, M., Ripepi, V., Bernabei, S., Ruoppo, A., Monteiro, M. J. P. F. G., Marques, J. P., et al. *Astrophys. Sp. Sci.* 2010, 328, 109
- Mashonkina, L., Gehren, T., Shi, J.-R., Korn, A. J. & Grupp, F. 2011, *A&A*, 528, 87
- Mayor, M., Pepe, F., Queloz, D., Bouchy, F., Rupprecht, G., Lo Curto, G., et al. 2003, *The Messenger*, 114, 20
- Meléndez, J. 2013, arXiv:1307.5274 (to appear in *Setting the scene for Gaia and LAMOST*, *Proc. IAU Symposium No. 298*)
- Pogodin, M. A., Hubrig, S., Yudin, R. V., Schöller, M., González, J. F. & Stelzer, B. 2012, *AN*, 333, 594
- Przybilla, N. & Butler, K. 2004, *ApJ*, 610, L61
- Przybilla, N., Butler, K., Becker, S.R., Kudritzki, R.P., Venn, K.A. 2000, *A&A*, 359, 1085
- Steenbock, W. & Holweger, H. 1984, *A&A*, 130, 319
- Turcotte, S. 2002, *ApJ*, L129
- Venn, K. A., Lambert, D. L. 1990, *ApJ*, 363, 234
- Vernet, J., Dekker, H., D'Odorico, S. D., Kaper, L., Kjaergaard, P., Hammer, F., et al. 2011, *A&A*
- Vieira, S. L. A., Corradi, W. J. B., Alencar, S. H. P., Mendes, L. T. S., Torres, C. A. O., Quast, G. R., Guimarães, M. M., da Silva, L. 2003, *AJ*, 126, 2971
- Wade, G. A., Bagnulo, S., Drouin, D., Landstreet, J. D. & Monin, D. 2007, *MNRAS*, 376, 1145
- Wiese, W.L., Fuhr, J.R., & Deters, T.M. 1996, *J. Phys. & Chem. Ref. Data*, Mon. 7

APPENDIX A: ONLINE MATERIAL

The online material gives wavelengths, measured equivalent widths, oscillator strengths, and lower excitation potentials for individual lines. References to original papers may be found in Tables 4 and A1 of Paper III. The online file is plain ascii and machine readable. The subset of weaker lines used for abundances are marked with an asterisk. The stronger lines were used for the microturbulence determination. Additional information is provided on the choice of oscillator strengths, and the relation of the adopted to the solar abundance.

Table A1: Sample of online material.

Sodium

Na I - $\text{Log}(\text{Na}/\text{N}_{\text{tot}}) = -5.89 \pm 0.1$. Results from the 4 weakest lines adopted. The solar value is -5.80 . Sodium is solar to within the errors.

Wavelen	W[mÅ]	log(W)	log(gf)	Chi(eV)	LogN/Ntot
4497.657*	12.9	1.11	-1.560	2.100	-5.99
4668.559*	29.5	1.47	-2.250	2.100	-5.88
5682.633	82.8	1.92	-0.700	2.100	-5.63
5688.205	110.0	2.04	-1.400	2.100	-5.56
5889.951	357.0	2.55	0.108	0.000	-5.64
5895.924	308.0	2.49	-0.194	0.000	-5.53
6154.226*	22.7	1.36	-1.547	2.100	-5.76
6160.747*	28.5	1.45	-1.246	2.100	-5.93